Volume 1 | Number 1 | Jan 2013 | Pages 1–100

Journal of
Materials Chemistry A

Materials for energy and sustainability
www.rsc.org/materialsA

Li+

e-

e-

Li+

Li+

Li+

ROYAL SOCIETY
OF CHEMISTRY

ROYAL SOCIETY
OF **CHEMISTRY**

www.rsc.org/materialsA

Journal Name

ARTICLE

Conformal and Highly Adsorptive Metal-Organic Framework Thin Films on Fibers: Fiber@ALD@MOF Structures Using Sonication-Enhanced Layer-by-Layer Growth on ALD Al2O3-Coated Polymer Fiber Mats

Junjie Zhao,[a] Bo Gong,[a] William T. Nunn,[a] Paul C. Lemaire,[a] Eric C. Stevens,[a] Fahim I. Sidi,[a] Philip S. Williams,[a] Christopher J. Oldham,[a] Howard J. Walls,[b] Sarah D. Shepherd,[b] Matthew A. Browe,[c] Gregory W. Peterson,[c] Mark D. Losego,[d] and Gregory N. Parsons*[a]

Integration of metal-organic frameworks (MOFs) on textiles shows promise for enabling facile deployment and expanding MOF applications. While MOFs deposited on flat substrates can show relatively smooth surface texture, most previous reports of MOFs integrated on fibers show poor conformality with many individual crystal domains. Here we report a new low-temperature (<70°C) method to deposit uniform and smooth MOF thin films on fiber surfaces using an energy enhanced layer-by-layer (LbL) method with an ALD Al2O3 nucleation layer. Cross-sectional TEM images show a well-defined core@shell structure of the MOF-functionalized fiber, and SEM shows a flat MOF surface texture. We analyze the thickness and mass increase data of LbL HKUST-1 MOF thin films on ALD-coated polypropylene fibers and find the growth rate to be 288~290 $ng \cdot cm^{-2}$ per LbL cycle. Unlike planar LbL MOF embodiments where adsorption capacities are difficult to quantify, the large volume quantity on a typical fiber mat enables accurate surface area measurement of these unique MOF morphologies. After 40 LbL cycles the MOFs on fibers exhibit N_2 adsorption BET surface areas of up to 93.6 $m^2/g_{MOF+fiber}$ (~535 m^2/g_{MOF}) and breakthrough test results reveal high dynamic loadings for NH_3 (1.37 $mol_{NH3}/kg_{MOF+fiber}$) and H_2S (1.49 $mol_{H2S}/kg_{MOF+fiber}$). This synthesis route is applicable to many polymer fibers, and the fiber@ALD@MOF structure is promising for gas filtration, membrane separation, catalysis, chemical sensing and other applications.

Introduction

Metal-organic frameworks (MOFs) are crystalline organic/inorganic materials consisting of nanoscale metal ions or cluster building blocks coordinated by organic linkers. MOFs exhibit large surface area and high porosity,[1] and many allow for post-synthetic chemical modification.[2–4] Utilizing these characteristics, MOFs have been applied to gas adsorption and storage,[5–8] separations,[9–11] and catalysis.[12–16] However, since MOFs are generally synthesized in the form of insoluble powders, methods for depositing MOF thin films are in high demand for applications such as adsorptive gas filters, smart membranes, chemical sensors and catalytic coatings.[17,18] Integration of MOFs into application-oriented configurations could also enable new device fabrication and simplify their deployment, pushing forward the commercialization of MOFs.

The layer-by-layer (LbL) method (or so-called "liquid phase epitaxy") generates thin MOF coatings of defined thickness with good homogeneity.[19,20] This synthetic approach is advantageous for controlling MOF structural interpenetration,[21] and has been used to build chemical sensors[22] and photo-switches for molecule release[23]. While most studies of the LbL method are based on planar substrate surfaces, including SAM surfaces on Au substrates,[24–27] silicon[20,22] and alumina substrates[20], little is known about the LbL process on fibers.

In most examples, even relatively modest MOF loading requires substrates selected specifically from carboxylic-group-consisting polymers (polyester[28] and silk fibers[29]), presumably to help promote MOF nucleation. For example, polyester fibers can be enriched with -COOH surface groups using polyvinylamine and bromoacetic acid sequentially to improve MOF growth.[28] MOFs formed on silk via LbL method appear as isolated crystals with a rough surface texture.[29] Until recently,[30] very few reports quantify BET surface areas or gas

adsorption capacities of MOFs on fibers, and no reports are available that analyze LbL MOFs on fibers.
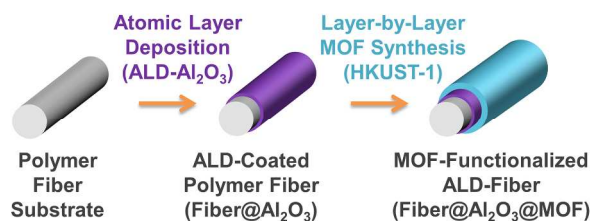
Scheme 1. Schematic of the synthesis route. Polymer fiber substrates were coated with 50 cycles of ALD-Al$_2$O$_3$, forming a core@shell structure of "Fiber@Al$_2$O$_3$". HKUST-1 MOF thin film was grown onto ALD-coated polymer fibers via layer-by-layer synthesis method.

Our recent work[30] introduced atomic layer deposition (ALD) as a MOF nucleation layer to dramatically improve solvothermal MOF growth on various polymer fibrous materials. Based on self-limiting reactions, ALD enables thin film coatings on complex 3D surfaces with a control of thickness at the sub-nanometer scale.[31] With abundant hydroxyl groups, ALD coatings improve the wettability of hydrophobic polymers,[32] and also provide anchoring sites for the metal-containing units in MOFs.[20] In this work, we show that ALD layers on fibers also promote LbL MOF growth, yielding very uniform and smooth MOF thin films on flexible polymer fibers.

Experimental

Nonwoven fiber mat materials

Nonwoven polypropylene (PP), polyethylene terephthalate (PET) and cotton fiber mats were used as received from Nonwovens Cooperative Research Center (NCRC), North Carolina State University. Fiber diameters of PP, PET, and cotton fiber mats are 0.6μm ~ 9.0μm, 33μm ~ 35μm and 13μm ~ 16μm respectively.

Atomic layer deposition (ALD) of Al$_2$O$_3$

Nonwoven fiber mats were coated with Al$_2$O$_3$ by ALD using a homemade hot-wall viscous-flow vacuum reactor (Figure S1). Deposition temperature was kept at 60°C, and pressure was ~1Torr. A typical ALD Al$_2$O$_3$ cycle started with trimethyl-aluminum (TMA, 98% STREM Chemicals, Inc.) dose for 1s and subsequent N$_2$ purge for 30s. After TMA dose and N$_2$ purge, deionized water was dosed to the chamber for 1s, followed with 60s of N$_2$ purge. 50 cycles of ALD Al$_2$O$_3$ were selected as the standard coating thickness for layer-by-layer MOF growth.

Layer-by-layer (LbL) growth of HKUST-1 MOF on fibrous materials

1mM 1,3,5-benzenetricarboxylic (BTC, 98%, Acros Organics) acid and 1mM copper acetate monohydrate (99%, Sigma Aldrich) were dissolved separately in two vessels with 150 mL ethanol. Precursor solutions and rinsing solvent (ethanol) were placed in a sonicated water bath during the LbL process. In a typical LbL cycle, non-woven fiber substrates were dipped in BTC solution for 5 minutes, followed with ethanol rinse for 1 minute. The substrates were then transferred to Cu(OAc)$_2$ solution for 5 minutes and subsequently rinsed in ethanol for 1

minute. During each transfer between vessels, the samples were dried in air for ~10 s. Precursor solutions were refreshed every 10 cycles to avoid a temperature effect when the sonication bath became heated. We observed heated sonication (>70°C) led to poor quality of MOF thin films. The rinse solution was refreshed every 4 cycles to maintain cleanliness. A good rinse process is critical for fully removing any unreacted species and/or unattached nuclei and maintaining controlled LbL growth.

Materials characterization

Scanning electron microscopy (SEM) and energy dispersive X-ray analysis (EDX) were performed on a JEOL JSM 6010 SEM. The synthesized fiber@ALD@MOF material structures were sputter-coated with a thin layer of Au-Pd (5~10nm) before SEM imaging. Microtomed fiber mats were imaged in cross section using a JEOL 2010F transmission electron microscope (TEM). Rigaku SmartLab X-ray diffraction (XRD) tool (Cu Kα X-ray source) was used for crystalline phase analysis. Fourier transform infrared spectrometer (FTIR, Thermo Scientific Nicolet 6700) was used to monitor LbL MOF growth on ALD-Al$_2$O$_3$ coated silicon wafers. Brunauer–Emmett–Teller (BET) surface area was measured on a Quantachrome Autosorb-1C surface area and pore size analyzer. Fiber@ALD@MOF samples were dried in vacuum ($\sim 1 \times 10^{-5}\ Torr$) at room temperature for 12h before BET measurement. An eleven-point nitrogen adsorption isotherm was measured for MOF-coated fiber mats at 77 K within P/P$_o$ range of 0.05~0.30.

Breakthrough test for NH$_3$ and H$_2$S

A custom-built rapid, micro-breakthrough system (shown in Scheme 2) was used for characterizing NH$_3$ and H$_2$S adsorption of our fiber@ALD@MOF materials. Challenge gas (NH$_3$ or H$_2$S) injected into a ballast was pressurized and subsequently mixed with a moisturized air stream to achieve the target concentration of 1000 mg/m^3 with 50% relative humidity (RH). The challenge gas mixture then flowed through an adsorbent column loaded with fiber@ALD@MOF material (~40 mg). The temperature of the adsorbent column was maintained at 20°C in a water bath. The downstream concentration of the challenge gas was detected with a continuously measuring gas chromatograph (HP5890 Series II) equipped with a photoionization detector for NH$_3$ (or a flame photometric detector for H$_2$S).[33]

Breakthrough data analysis

Dynamic loadings (DL in units of mol/kg) of NH$_3$ or H$_2$S on MOF-coated fibers were calculated from the breakthrough curves using the following equations.[33]

$$N_{feed} = \frac{C_{feed}F_{feed} \cdot t_{total}}{M_w} \qquad (1)$$

$$N_{out} = \int_0^{t_{total}} \frac{C_{out}F_{feed}}{M_w} dt \qquad (2)$$

$$DL = \frac{N_{feed} - N_{out}}{m_{ads}} \qquad (3)$$

N_{feed} is defined as the total moles of challenge gas flowing through the adsorbent, while N_{out} is the total moles of target gas detected in the effluent stream. C_{feed} and C_{out} (in g/m^3) are the concentrations of challenge gas in the feed and the downstream respectively. Feed flow rate (F_{feed}) has units of m^3/min, and

time (t) has units of min. M_w (g/mol) is the molecular weight of the challenge gas, and m_{ads} (kg) is the adsorbent mass.
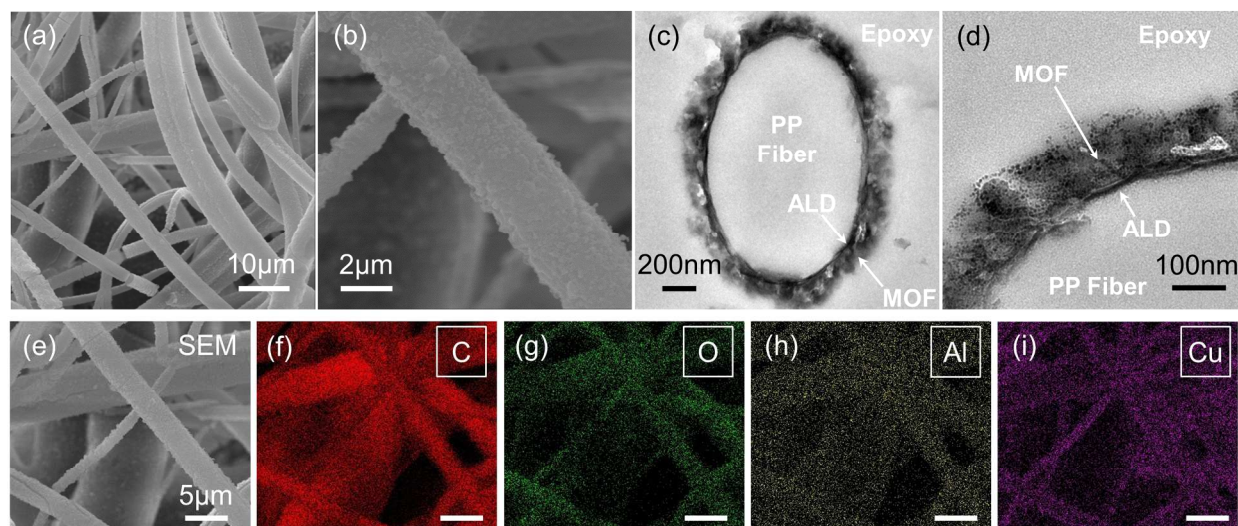
Figure 1. (a,b,e) SEM images for ALD-Al$_2$O$_3$-coated PP fibers with 40 cycles of LbL HKUST-1 MOF (PP@ALD@LbL40). (c, d) Cross-sectional TEM images for PP@ALD@LbL40 showing the core@shell structure. (f-i) Energy Dispersive X-ray analysis for PP@ALD@LbL40 showing the presence of carbon (f) from the polypropylene and the HKUST-1 MOF, oxygen (g) from the ALD Al$_2$O$_3$ and the HKUST-1 MOF, aluminum (h) from the ALD coating and copper (i) from the MOF.
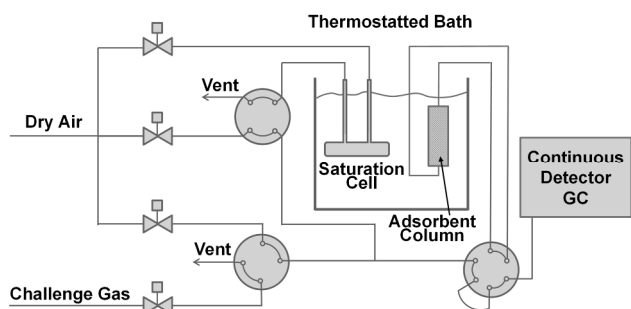
Scheme 2. Schematic of the rapid micro-breakthrough analysis system for NH$_3$ and H$_2$S breakthrough tests.

Results and Discussion

Conformal LbL MOF Thin Films Enabled by ALD-Al$_2$O$_3$ Nucleation Layer

Figure 1 displays SEM and TEM images showing the microscopic morphology of MOF thin films grown on ALD-Al$_2$O$_3$ coated polypropylene (PP) fibers. 50 cycles of ALD Al$_2$O$_3$ was deposited on PP fibers at 60 ℃, forming a Fiber@ALD core@shell structure (PP@ALD). Subsequently, 40 cycles of LbL HKUST-1 MOF was synthesized on top of the ALD coating, adding an extra shell layer to PP@ALD (shown in Scheme 1). We refer to these MOF-functionalized materials as PP@ALD@LbL40. Figures 1a and 1b show good uniformity and complete fiber coverage of the LbL MOF thin film. During solvothermal MOF film growth on ALD-coated fibers, MOF crystals may nucleate homogeneously within the fiber mat in the voids between fibers.[30] However, the LbL method shows only MOFs directly deposited on the fibers. Sufficient ethanol rinsing in sonication bath between dipping steps in LbL process can remove unreacted precursor molecules and/or unattached nuclei from the fiber mesh, ensuring MOF formation happens only on the reactive surface of the fibers. A high magnification SEM image shown in Figure 1b suggests the average MOF crystal size is ≤1 μm. In comparison, MOF crystals grown on ALD-coated PP fibers via solvothermal synthesis are typically >5 μm.[30] This indicates the LbL method is more advantageous in controlling the surface roughness of the MOF coating.

Figures 1c and d show cross-sectional TEM images of the PP@ALD@LbL40 core@shell structures. The well-defined thin layer (~10 nm thick) sandwiched between the fiber substrate and the thick coating corresponds to the ALD-Al$_2$O$_3$ thin film. The ALD growth rate (~2 Å/cycle) and the smoothness of the coating deposited at 60 ℃ are consistent with previous analysis of low temperature ALD on these fiber materials.[34] With abundant hydroxyl termination, this ALD layer is expected to facilitate MOF nucleation.[30] On top of the ALD coating, a layer with less uniform TEM contrast corresponds to the LbL HKUST-1 MOF thin film. This MOF layer exhibits good conformality, with an average thickness of 117 nm. The higher resolution TEM image in Figure 1d shows that the LbL MOF thin film is porous and consists of nanocrystals with dimensions of about 5 nm to 8 nm. Similar nanoparticles were also observed and reported by Wöll and co-workers for their work on LbL HKUST-1 coating on magnetic nanoparticles.[35] These nanoparticles are likely CuO produced from the HKUST-1 during electron beam irradiation in the TEM.

The energy dispersive X-ray analysis (EDX) images for PP@ALD@LbL40 are shown in Figures 1(f-i). The results show a uniform aluminum signal from the fibers, indicating the ALD Al$_2$O$_3$ coating is conformal and is fully maintained after MOF integration. Copper is also detected uniformly on the fibers, further confirming complete and uniform MOF coverage. Carbon is expected from the polypropylene and from the MOF organic linker (1,3,5-benzenetricarboxylic acid). The ALD thin

films and the MOF coatings are both likely to contribute to the oxygen signal detected by EDX.

To examine MOF nucleation mechanisms, we performed 20 MOF LbL cycles on PP fibers with and without Al_2O_3 ALD pretreatment. SEM images of these coated fibers are compared
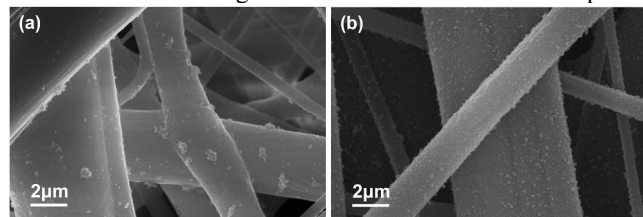
Figure 2. SEM images of (a) 20 cycles of LbL HKUST-1 MOF on untreated PP fibers and (b) 20 cycles of LbL HKUST-1 MOF on ALD-Al_2O_3-coated PP fibers (PP@ALD). MOF thin film grown on untreated PP substrate exhibits poor uniformity, while MOF coating on PP@ALD shows good conformality with complete coverage on fibers.

in Figure 2. PP fibers without an Al_2O_3 coating (Fig. 2a) exhibit non-uniform and patchy MOF growth, whereas MOFs grown PP@ALD fibers (Fig. 2b) are uniform and smooth. The improved nucleation and growth on the ALD-treated substrate is consistent with that reported for solvothermal MOF growth on polymer fibers.[30] Virgin PP fibers are devoid of reactive functional groups and, therefore, are relatively inert to MOF nucleation. Consequently, MOF nucleation likely occurs on random surface defects. Once the nucleation seed is attached to the untreated fiber, the MOF will continue to grow preferentially at this site leading to a patchy coverage.

Growth Rate of LbL HKUST-1 MOF on ALD Al_2O_3 Coatings

Figure 3a is an optical image showing the color change due to the growth of LbL MOFs on ALD-coated PP fiber mats. The ALD Al_2O_3 (50 cycles) does not change the visual color of the PP fiber substrate. With increased number of LbL cycles, the fiber mats transition from white to turquoise blue. If dried in vacuum, the MOF functionalized fiber mats would turn deep purple, consistent with the loss of water ligands on the copper paddle wheels, as observed for solvothermally prepared HKUST-1 MOFs during vacuum degassing. The X-ray diffraction data shown in Figure 3b further confirm the HKUST-1 crystal structure. The diffraction signal intensity increases with the number of LbL cycles.

To quantify the growth rate of the LbL process, we analyzed MOF film thickness using high-resolution cross-sectional TEM (Fig. 3c) and characterized the mass change vs. number of LbL cycles (Fig. 3d). Figure 3c shows the thickness of 0~40 cycles of LbL MOF coatings on ALD-Al_2O_3 coated PP fibers. For the TEM analysis, at least 5 cross-sectional images were collected for each sample type, and 5 data points were measured on each image. The MOF coating thickness increases linearly with the number of LbL cycles, and the slope corresponds to a growth rate of 3.0 nm/cycle. Using the reported density for HKUST-1 (0.96 $g·cm^{-3}$),[36] the change in thickness corresponds to a mass gain of ~288 $ng·cm^{-2}$/cycle. The thickness/cycle value we find is close to 2.634 nm, the periodicity of the HKUST-1 MOF unit cell in the [100] direction,[19,36] suggesting the LbL method produces one MOF "monolayer" per cycle. Previous results show HKUST-1 LbL growth on alumina to be ~2.5 nm/cycle.[20] Small differences in these values may point to subtle but important differences in the LbL growth reactions. We believe that more detailed studies of

half-cycle reaction saturation and effects of process conditions on MOF growth rate need to be performed to define true "layer by layer" deposition reaction conditions.
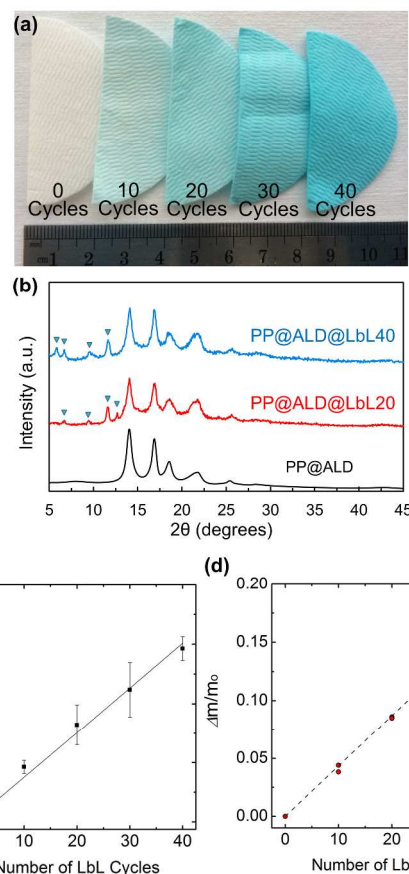

Figure 3. (a) Optical images of ALD-Al_2O_3-coated PP fibers with 0~40 cycles of LbL HKUST-1 MOF. (b) X-ray diffraction data of ALD-Al_2O_3-coated PP fibers with 0, 20, 40 cycles of LbL HKUST-1 MOF. Green triangles (▼) represent the peaks for HKUST-1 MOF. (c) Thickness of the MOF coating (0~40 LbL cycles) on ALD-Al_2O_3-coated PP fibers measured from cross-section TEM images. Error bars represent a 95% confidence interval based on 25 data points measured for each fiber mat. Solid line is a linear-fitted line to the data points. (d) Percent mass increase of LbL HKUST-1 MOF (0~40 cycles) based on the dry weight of the fiber substrates ($\Delta m/m_o$). Dashed line is a linear-fitted line to the data points.

We also measured the mass gain for different numbers of LbL cycles on ALD-coated PP fibers, and calculated percent mass increase ($\Delta m/m_o$) based on the dry mass of the substrates. The percent mass gain (Fig. 3d) also scales linearly with the number of LbL cycles, with a slope of 0.435% per cycle (or $4.35 \times 10^{-3} g_{MOF}/g_{fiber}$ per cycle). Considering the BET surface area of ALD-coated PP fibers is ~1.5 m^2/g, the mass gain corresponds to ~290 $ng·cm^{-2}$/cycle, showing excellent consistency between the mass gain and TEM thickness analysis results.

In addition to PP fibers, we studied the growth rate of LbL HKUST-1 thin films on ALD-Al_2O_3 coated silicon wafers by monitoring the characteristic peaks for carboxylate in Fourier transform infrared (FTIR) spectra. In a typical LbL cycle, Al_2O_3 coated silicon wafers were dipped sequentially in BTC and $Cu(OAc)_2$ ethanolic solutions for 1 hour, with 5-minute ethanol wash steps in between. FTIR spectra were collected for 1, 2, 4, 6, 8 and 10 cycles of LbL MOF growth. The

asymmetric (1645 and 1590 cm^{-1}) and symmetric (1450 and 1370 cm^{-1}) stretching vibration modes shown in Figure 4a
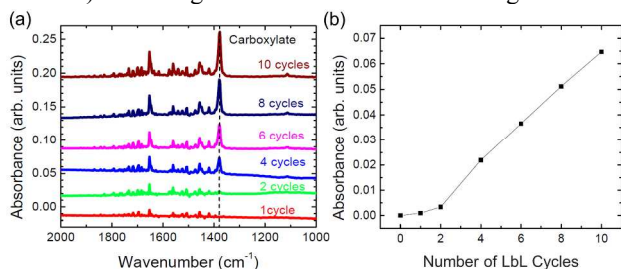
Figure 4. (a) Fourier transform infrared (FTIR) spectra for HKUST-1 thin films deposited on ALD-Al$_2$O$_3$ coated silicon wafers using layer-by-layer (LbL) method. Al$_2$O$_3$ coated silicon wafers were dipped sequentially in LbL precursor solutions for 1 hour with 5-minute ethanol wash steps in between. (b) Plot of IR absorbance at ~1370 cm^{-1} (carboxylate symmetric stretching vibrations) vs. number of LbL cycles. A linear increase was observed for the absorbance at ~1370 cm^{-1} after 2 LbL cycles.

represent the carboxylate linkers in the MOF thin films.[37] The absorbance of the carboxylate peak at 1370 cm^{-1} was plotted vs. number of LbL cycles in Figure 4b. A linear increase in IR absorbance at 1370 cm^{-1} was observed after the first 2 LbL cycles, indicating a layer-by-layer growth fashion after the initial nucleation delay.

Adsorption Capacity of Fiber@ALD@MOF

Figure 5 shows the BET surface area of PP@ALD@MOF fibers (determined from BET using an eleven point N$_2$ isotherm, p/p_o=0.05~0.30, at 77K) plotted versus number of MOF LbL cycles. ALD Al$_2$O$_3$ coated PP fiber mats had a surface area of ~1.5 m^2/g. The MOF coating added substantial surface area to the substrate, with values exceeding 93 m^2/g$_{MOF+fiber}$ after 40 LbL cycles. Note that this surface area is normalized to the total mass of MOF+fiber, so the surface area per unit mass of MOF is substantially larger. Following procedures developed previously,[30] we analyzed the MOF mass fraction on fiber@ALD@MOF samples using careful drying and weighing protocols before and after MOF LbL growth. With this method, after 40 LbL cycles the MOF mass fraction is ~17%, giving a surface area of ~535 m^2/g$_{MOF}$. While the surface area in the range of ~500 m^2/g$_{MOF}$ shows good porosity, the value is still ~2× smaller than typical surface area for bulk HKUST-1 crystals prepared via solvothermal synthesis. The trend in surface area vs. LbL cycle in Figure 5 shows the surface area increases non-linearly, with a larger increase during later LbL cycles. This indicates that the surface area of the growing MOF crystals improves as growth proceeds, suggesting that MOF thin film deposited in initial LbL cycles may be amorphous or have a poorer crystallinity than that coated in subsequent LbL cycles.

We also evaluate the adsorption capacity of the Fiber@ALD@MOF materials for hazardous gases via breakthrough tests. Figure 6a shows the NH$_3$ breakthrough curves for 0, 20, 40 cycles of LbL HKUST-1 MOF on ALD-coated PP fibers. Ammonia concentration detected downstream changes as a function of time, and breakthrough is defined as the time when the downstream concentration reaches 5% of the feed concentration (C$_o$). Without MOF coating, PP@ALD fibers show immediate breakthrough when exposed to ammonia, consistent with zero NH$_3$ adsorption. As the MOF mass increases, breakthrough time increases, indicating a larger adsorption capacity. PP@ALD@LbL40 fiber mat exhibits breakthrough time of ~700 min/g$_{MOF+fiber}$ and ~4200 min/g$_{MOF}$,

which is ~80% of the previously reported values for MOF-fiber mats prepared via solvothermal method.[30]
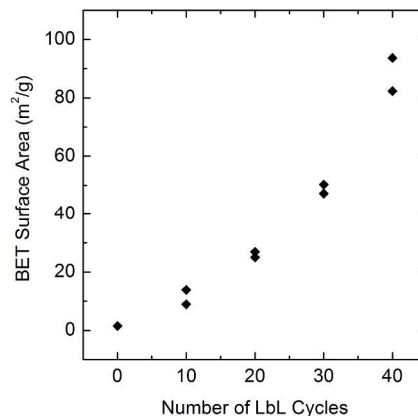
Figure 5. Brunauer-Emmett-Teller (BET) surface area (in units of m^2/g$_{MOF+Fiber}$) of ALD-Al$_2$O$_3$-coated PP fibers with 0~40 cycles of LbL HKUST-1 MOF.
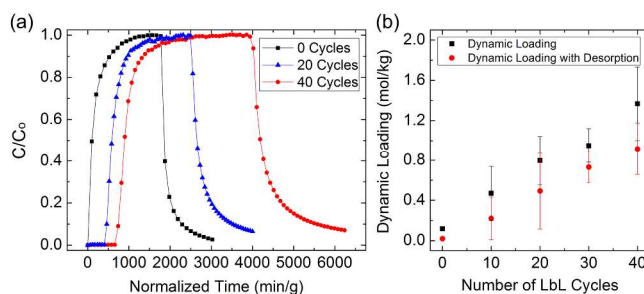
Figure 6. (a) NH$_3$ breakthrough curves for ALD-coated PP fiber mat with no LbL MOF (■), 20 cycles of LbL MOF (▲) and 40 cycles of LbL MOF (●). (b) NH$_3$ dynamic loading on ALD-coated PP fiber mats with 0, 20, 40 cycles of LbL MOF. Square points (■) were calculated based on the corresponding breakthrough curve before saturation, and circle points (●) were calculated with the desorption part. Error bar represents standard deviation.

Dynamic loadings are calculated for both saturation adsorption with and without desorption. Saturation dynamic loadings (without desorption) represents the total sorption capacity, which includes the physisorption and chemisorption capacity. Dynamic loading with desorption reveals the amount of NH$_3$ retained in the adsorbent even after the feed gas is terminated, i.e. the amount of NH$_3$ that is chemisorbed. Results from dynamic loading with and without desorption are shown in Figure 6b. For both measurements, the NH$_3$ dynamic loading increase almost linearly with the number of LbL cycles. With 40 LbL cycles, PP@ALD@LbL40 exhibits a dynamic loading (without desorption) of 1.37 mol$_{NH3}$/kg$_{MOF+fiber}$, equivalent to 7.63 mol$_{NH3}$/kg$_{MOF}$. With no MOF present, the PP@ALD samples show nearly zero (0.12 mol$_{NH3}$/kg$_{fiber}$) dynamic NH$_3$ loading without desorption. Dynamic loading of 7.63 mol$_{NH3}$/kg$_{MOF}$ agrees well with reported data for bulk HKUST-1 powder (6.6~8.9 mol$_{NH3}$/kg$_{MOF}$),[38] and similar to values reported for solvothermal MOFs grown on fibers.[30] With consideration of desorption, PP@ALD@40 can still retain 0.92 mole of ammonia per kilogram of MOF+fiber.

In addition to ammonia adsorption, we also tested PP@ALD@LbL40 fiber mats for H$_2$S absorption. The dynamic loading without desorption is up to 1.49 mol$_{H2S}$/kg$_{MOF+fiber}$ (or

9.46 mol$_{H2S}$/kg$_{MOF}$), and that dynamic loading with desorption is up to 1.44 mol$_{H2S}$/kg$_{MOF+fiber}$.
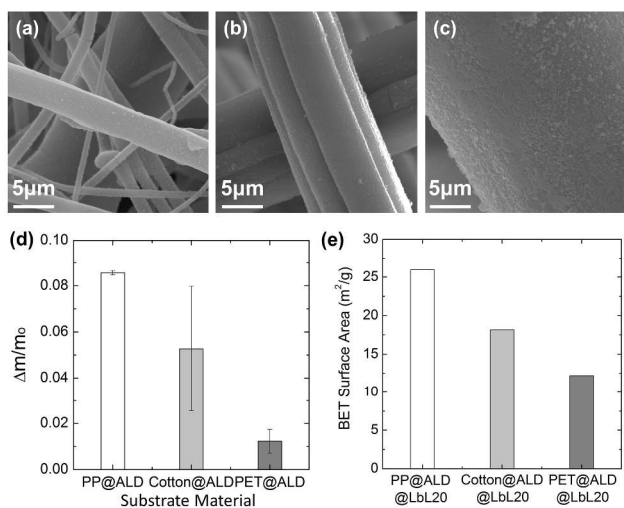
Figure 7. (a-c) SEM images of 20 cycles of LbL HKUST-1 MOF grown on ALD-Al$_2$O$_3$-coated polypropylene (a), polyethylene terephthalate (b) and cotton (c). (d) Percent mass gain for 20 LbL cycles on PP@ALD, PET@ALD and Cotton@ALD. (e) BET surface area of PP@ALD@LbL20, PET@ALD@LbL20 and Cotton@ALD@LbL20.

LbL MOF on ALD-coated PET and Cotton Fibers

The Fiber@ALD@MOF core@shell structure is not limited to polypropylene substrates. We also deposited LbL MOF thin films on ALD-coated polyethylene terephthalate (PET) and cotton non-woven fiber mats. Figures 7a-c compare the microscopic morphology of the LbL MOF thin films grown on PP@ALD, PET@ALD and Cotton@ALD. MOF coating on these substrates all exhibits good uniformity, high coverage and smooth surface texture. Figure 7d shows percent mass increase for 20 LbL cycles on different polymer substrates. We find the percent mass gain data decreases as the diameter of the substrate fiber increases. Assuming the MOF thickness increase per cycle (Δh, in units of cm/cycle) is same for different fibers, the percent mass gain will be inversely proportional to the fiber diameter (Eqn. 4).

$$\frac{\Delta m}{m_o} = \frac{\rho_{MOF} \cdot V_{MOF}}{\rho_{fiber} \cdot V_{fiber}} = \frac{\rho_{MOF} \cdot (\Delta h \cdot SA_{fiber})}{\rho_{fiber} \cdot (SA_{fiber} \cdot \frac{d_{fiber}}{4})} = \frac{4 \, \rho_{MOF}}{\rho_{fiber}} \cdot \frac{\Delta h}{d_{fiber}} \quad (4)$$

where Δm is mass increase per cycle due to MOF deposition in units of mg/cycle, m_o is the substrate weight of ALD-coated fibers in mg, ρ_{MOF} and ρ_{fiber} (g·cm^{-3}) are the densities of the MOF thin film and the ALD-coated fibers respectively, SA_{fiber} is the surface area of the fibers in cm^2, d_{fiber} is the diameter of the fibers in cm. The trend predicted by equation (4) is consistent with results in Figure 7d, showing decreasing MOF mass fraction for cotton and PET substrates with larger average fiber diameter.   The total BET surface area (m^2/g$_{MOF+fiber}$) shown in Figure 7e also scales with MOF mass fraction, indicating that the MOF surface area on these substrates is similar to the MOFs formed on polypropylene.

Conclusions

We demonstrate fabrication of fiber@ALD@MOF core@shell structures with conformal and smooth MOF surfaces using a combination of controlled inorganic atomic layer deposition and MOF layer-by-layer synthesis on natural and synthetic polymer fibers. We use ALD Al$_2$O$_3$ thin film as a nucleation layer for LbL HKUST-1 MOF crystals, and SEM and cross-sectional TEM images confirm good uniformity and high fiber coverage of the MOF thin films. After 40 LbL cycles on Al$_2$O$_3$-coated PP fibers, the BET surface area for the MOF thin films is ~535 m^2/g$_{MOF}$. Although the value is not as high as crystals prepared via solvothermal methods, we expect the MOF quality and surface area per gram to increase as growth proceeds further. Analysis of the MOF coating thickness shows the growth rate is 3.0 nm/cycle. Calculation based on both the thickness and the percent mass gain data reveal a consistent value of 288~290 ng·cm^{-2}/cycle for the growth rate of LbL HKUST-1 on ALD-coated PP fibers. Furthermore, the PP@ALD@MOF fiber mats formed by ALD/LbL have high adsorption capacity for NH$_3$ and H$_2$S. The dynamic loadings of the MOF thin film are comparable to those of bulk MOF powder, indicating the good quality of the MOF coating. We also confirm this synthesis route is applicable to other polymer fibers, such as PET and cotton. In addition to hazardous gas removal, this fiber@ALD@MOF structure is also promising for catalysis, chemical sensing and many other applications.

Notes and references

[a] Department of Chemical and Biomolecular Engineering, North Carolina State University, 911 Partners Way, Raleigh, NC 27695, United States.

[b] RTI International, 3040 East Cornwallis Road, Research Triangle Park, NC 27709, U.S.A.

[c] Edgewood Chemical Biological Center, 5183 Blackhawk Road, Aberdeen Proving Ground, MD 21010, United States.

[d] School of Materials Science and Engineering, Georgia Institute of Technology, 771 Ferst Dr. NW, Atlanta, GA 30332, U.S.A.

1   H. Furukawa, K. E. Cordova, M. O'Keeffe, and O. M. Yaghi, *Science*, 2013, **341,** 1230444.

2   M. Kim, J. F. Cahill, H. Fei, K. A. Prather, and S. M. Cohen, *J. Am. Chem. Soc.*, 2012, **134,** 18082–18088.

3   W. M. Bloch, A. Burgun, C. J. Coghlan, R. Lee, M. L. Coote, C. J. Doonan, and C. J. Sumby, *Nat. Chem.*, 2014, **6,** 906–912.

4   C. K. Brozek and M. Dincă, *Chem Soc Rev*, 2014, **43,** 5456–5467.

5   N. L. Rosi, J. Eckert, M. Eddaoudi, D. T. Vodak, J. Kim, M. O'Keeffe, and O. M. Yaghi, *Science*, 2003, **300,** 1127–1129.

6   D. Britt, D. Tranchemontagne, and O. M. Yaghi, *Proc. Natl. Acad. Sci. U. S. A.*, 2008, **105,** 11623–11627 (2008).

7   L. J. Murray, M. Dinca, and J. R. Long, *Chem. Soc. Rev.*, 2009, **38,** 1294–1314.

8   K. Sumida, D. L. Rogow, J. A. Mason, T. M. McDonald, E. D. Bloch, Z. R. Herm, T.-H. Bae, and J. R. Long, *Chem. Rev.*, 2012, **112,** 724–781.

9   L. Pan, D. H. Olson, L. R. Ciemnolonski, R. Heddy, and J. Li, *Angew. Chem. Int. Ed.*, 2006, **45,** 616–619.

10   J.-R. Li, R. J. Kuppler, and H.-C. Zhou, *Chem. Soc. Rev.*, 2009, **38,** 1477–1504.

11   S. Couck, J. F. M. Denayer, G. V. Baron, T. Remy, J. Gascon, and F. Kapteijn, *J. Am. Chem. Soc.*, 2009, **131,** 6326.

12   J. Lee, O. K. Farha, J. Roberts, K. A. Scheidt, S. T. Nguyen, and J. T. Hupp, *Chem. Soc. Rev.*, 2009, **38,** 1450–1459.

13   C. Wang, Z. Xie, K. E. deKrafft, and W. Lin, *J. Am. Chem. Soc.*, 2011, **133,** 13445–13454.

14   Y. Xie, T.-T. Wang, X.-H. Liu, K. Zou, and W.-Q. Deng, *Nat. Commun.*, 2013, **4,** 1960.

15   D. Sun, Y. Fu, W. Liu, L. Ye, D. Wang, L. Yang, X. Fu, and Z. Li, *Chem. – Eur. J.*, 2013, **19,** 14279–14285.

16   S. Wang, W. Yao, J. Lin, Z. Ding, and X. Wang, *Angew. Chem. Int. Ed.*, 2014, **53,** 1034–1038.

17   L. Bo and R. A. Fischer, *Sci. China-Chem.*, 2011, **54,** 1851–1866.

18   D. Bradshaw, A. Garai, and J. Huo, *Chem. Soc. Rev.*, 2012, **41,** 2344–2381.

19   C. Munuera, O. Shekhah, H. Wang, C. Wöll, and C. Ocal, *Phys. Chem. Chem. Phys.*, 2008, **10,** 7257–7261.

20   V. Stavila, J. Volponi, A. M. Katzenmeyer, M. C. Dixon, and M. D. Allendorf, *Chem. Sci.*, 2012, **3,** 1531–1540.

21   O. Shekhah, H. Wang, M. Paradinas, C. Ocal, B. Schuepbach, A. Terfort, D. Zacher, R. A. Fischer, and C. Wöll, *Nat. Mater.*, 2009, **8,** 481–484.

22   G. Lu and J. T. Hupp, *J. Am. Chem. Soc.*, 2010, **132,** 7832.

23   L. Heinke, M. Cakici, M. Dommaschk, S. Grosjean, R. Herges, S. Bräse, and C. Wöll, *ACS Nano*, 2014, **8,** 1463–1467.

24   O. Shekhah, H. Wang, S. Kowarik, F. Schreiber, M. Paulus, M. Tolan, C. Sternemann, F. Evers, D. Zacher, R. A. Fischer, and C. Wöll, *J. Am. Chem. Soc.*, 2007, **129,** 15118–15119.

25   O. Shekhah, H. Wang, D. Zacher, R. A. Fischer, and C. Wöll, *Angew. Chem. Int. Ed.*, 2009, **48,** 5038–5041.

26   B. Liu, M. Ma, D. Zacher, A. Betard, K. Yusenko, N. Metzler-Nolte, C. Wöll, and R. A. Fischer, *J. Am. Chem. Soc.*, 2011, **133,** 1734–1737.

27   H. K. Arslan, O. Shekhah, J. Wohlgemuth, M. Franzreb, R. A. Fischer, and C. Wöll, *Adv. Funct. Mater.*, 2011, **21,** 4228–4231.

28   M. Meilikhov, K. Yusenko, E. Schollmeyer, C. Mayer, H.-J. Buschmann, and R. A. Fischer, *Dalton Trans.*, 2011, **40,** 4838–4841.

29   A. R. Abbasi, K. Akhbari, and A. Morsali, *Ultrason. Sonochem.*, 2012, **19,** 846–852.

30   J. Zhao, M. D. Losego, P. C. Lemaire, P. S. Williams, B. Gong, S. E. Atanasov, T. M. Blevins, C. J. Oldham, H. J. Walls, S. D. Shepherd, M. A. Browe, G. W. Peterson, and G. N. Parsons, *Adv. Mater. Interfaces*, 2014, **1,** 1400040.

31   G. N. Parsons, S. M. George, and M. Knez, *MRS Bull.*, 2011, **36,** 865–871.

32   G. K. Hyde, G. Scarel, J. C. Spagnola, Q. Peng, K. Lee, B. Gong, K. G. Roberts, K. M. Roth, C. A. Hanson, C. K. Devine, S. M. Stewart, D. Hojo, J.-S. Na, J. S. Jur, and G. N. Parsons, *Langmuir*, 2010, **26,** 2550–2558.

33   T. G. Glover, G. W. Peterson, B. J. Schindler, D. Britt, and O. Yaghi, *Chem. Eng. Sci.*, 2011, **66,** 163–170.

34   J. S. Jur, J. C. Spagnola, K. Lee, B. Gong, Q. Peng, and G. N. Parsons, *Langmuir*, 2010, **26,** 8239–8244.

35   M. E. Silvestre, M. Franzreb, P. G. Weidler, O. Shekhah, and C. Wöll, *Adv. Funct. Mater.*, 2013, **23,** 1210–1213.

36   S. S. Chui, *Science*, 1999, **283,** 1148–1150.

37   C. Petit, B. Mendoza, and T. J. Bandosz, *Chemphyschem*, 2010, **11,** 3678–3684.

38   G. W. Peterson, G. W. Wagner, A. Balboa, J. Mahle, T. Sewell, and C. J. Karwacki, *J. Phys. Chem. C*, 2009, **113,** 13906–13917.

Journal of Materials Chemistry A Accepted Manuscript

Table of Contents

Fiber@ALD@MOF structures fabricated via ALD and layer-by-layer MOF synthesis show good conformality and high adsorption capacity.